PERGAMON

International Journal of Solids and Structures 38 (2001) 6787–6803

INTERNATIONAL JOURNAL OF SOLIDS and STRUCTURES

www.elsevier.com/locate/ijsolstr

Displacement-based mode separation of strain energy release rates for interfacial cracks in bi-material media

Srinivasan Sridharan *

Department of Civil Engineering, Washington University in St. Louis, Campus Box 1130, One Brooking Drive, St. Louis, MO 63130-4899, USA

Received 21 August 2000

Abstract

A new method of determining the opening and shearing modal components of the total strain energy release rate during crack extension is described. The method is based on suppressing one mode at a time over a certain length downstream of the crack tip (b) and letting the crack extend by a certain amount (Δa) with this condition maintained over the length $b + \Delta a$. The modal components thus obtained, however, do not add up to the total strain energy release rate (G) and are also dependent on the length b. These approximate values and the total strain energy release rate are used as a starting point to obtain the modal components that would add up to the total G and are not associated with any particular b. Numerical examples of cracks in homogeneous media and those along bi-material interfaces are presented to illustrate the methodology and the relative independence of the results of the mesh size and the length of Δa selected. It appears that the modal components thus obtained are rationally based global parameters which are determinable without considering local crack-tip stress distribution.

Keywords: Strain energy release rate; Mode separation; Opening and shearing modes; Displacement-based approach; Bi-material interfaces

1. Introduction

Prediction of delamination growth along a bi-material interface is currently based on semi-empirical procedures. There appears to be no well established, rational procedure for the computation of the modal components G_{I} and G_{II} of strain energy release rate in the case of bi-material cracks to help assess the risk of delamination growth. This problem has assumed greater urgency in recent times because of the extensive use of sandwich composites in ship structures in which a frequent mode of failure is separation of the stiff facing sheets and the relatively soft core. In the present study a consistent displacement-based approach is presented for achieving the mode separation. Though based on the approach previously presented by Johnson and Sridharan (1999), the present approach corrects for some inconsistencies thereof.

* Fax: +1-314-935-4338.

E-mail address: ssrid@seas.wust1.edu (S. Sridharan).

0020-7683/01/$ - see front matter
PII: S0020-7683(01)00050-6

Nomenclature

E_{11}, E_{22}, E_{33}	modulus of elasticity of a composite lamina in the fiber, in-plane transverse and out of plane normal directions respectively.
G	total strain energy release rate
G_1, G_2	opening and shear modal components of G as given by the crack-closure integrals
G_{I}, G_{II}	opening and shear modal components of G as given by the displacement-based method
G^a_{I}, G^a_{II}	values of G_{I}, G_{II} before correction
G_{12}, G_{13}, G_{23}	in-plane shear modulus and out of plane shear moduli
a	length of the crack
b	distance over which the crack is conditioned prior to crack extension
$\tilde{h}$	mesh size in the direction of the crack
$\tilde{u}$, $\tilde{v}$	relative crack displacements in the opening and shearing mode
Δa	crack extension
Π	total potential energy of the structure
σ_y, τ_{xy}	normal and shearing stresses over the crack surface prior to crack extension

1.1. Mode separation techniques: a commentary

1.1.1. Crack-closure integrals

Crack-closure integrals are a popular tool for the computation of total strain energy release rates (SERR) as well as its modal components and are attributed to Irwin (1957). For the interface crack geometry shown in Fig. 1, the energy release rate, G, can be expressed in the form:

$$G = \operatorname*{Lim}_{\Delta a \to 0} \frac{1}{2\Delta a} \int_0^{\Delta a} \sigma_y(x)\tilde{v}(x)\mathrm{d}x + \operatorname*{Lim}_{\Delta a \to 0} \frac{1}{2\Delta a} \int_0^{\Delta a} \tau_{xy}(x)\tilde{u}(x)\mathrm{d}x \tag{1}$$

where σ_y and τ_{xy} are the stresses upstream of the crack tip, $\tilde{u}$ and $\tilde{v}$ are the relative sliding and opening displacements between points facing each other on the crack faces after the crack extension and Δa is the crack extension. The first term gives the contribution of the opening mode (mode I), G_1 and the second term is that of the shear mode (mode II), G_2. (Note arabic subscripts 1 and 2 have been used for the results obtained from crack-closure integrals, the roman ones being reserved for displacement-based values.) In the context of finite element analysis, this can be expressed in terms of nodal forces on the upstream of the crack prior to crack extension and the corresponding crack opening displacements after the crack extension (Rybicki and Kanninen, 1977; Raju et al., 1998).

For a bi-material crack the crack-closure integrals have been shown not to converge (Sun and Jih, 1987) although the sum $G = G_1 + G_2$ does converge and is well defined. A number of attempts have been made to extract reasonable estimates of the modal contributions using crack-closure integrals. One of these methods involves inserting a thin homogeneous layer of resin between the layers forming the interface and placing the crack with in it (Atkinson, 1977). This involves considerable additional computational effort to retrieve the stresses and the SERR components, as the stresses may retain considerable mesh-sensitivity if the resin layer is extremely thin. Davidson (1994) has suggested changing the Poisson ratio of one of the layers so that a key bi-material parameter ϵ which is the source oscillatory behavior becomes zero. The implications of such a change are not clear and the consistent accuracy of the results obtained have not been established. It has been observed that a relatively large crack extension retrieves results which are physically meaningful (Davidson, 1994; Rice, 1968) and helps to mitigate the influence of oscillatory nature of stress variations

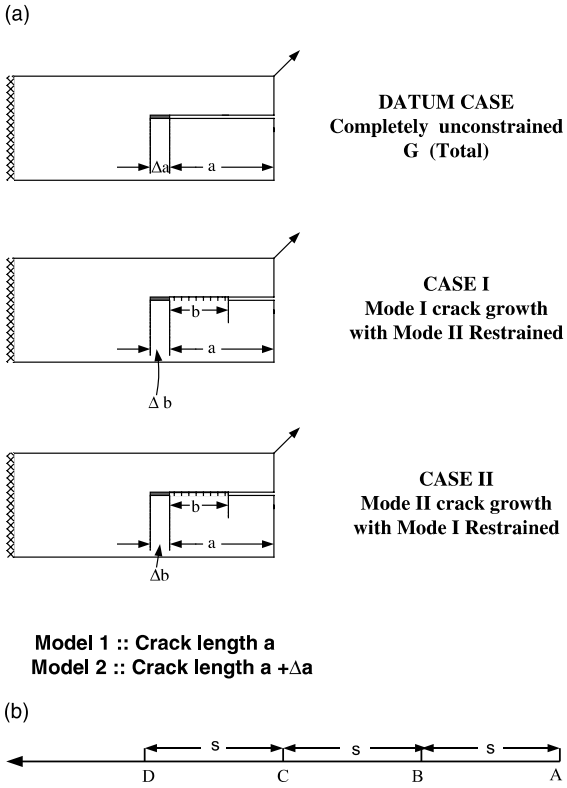

Fig. 1. (a) The three models and the corresponding scenarios of crack extension ($\Delta a = \Delta b$). (b) Numerical integration scheme (A, the origin is at the free end and X runs towards the crack tip).

near the crack tip. Finally, there have been approaches where the oscillatory component can be identified and discarded to obtain consistent values of mode mixity (Beuth, 1996). Even though such an approach would lead to results which are not mesh-sensitive, the validity of the results are open to question. For a problem involving two dissimilar isotropic materials, this approach would lead to $G_1 = G_2$ [5] – a result which will be seen to be erroneous.

1.2. Displacement-based approach

A displacement-based method has been developed for obtaining the strain energy release rate (SERR, G) and its modal components (G_{I} and G_{II}) by Johnson and Sridharan recently for two-dimensional problems (Johnson and Sridharan, 1999). A brief description of the technique is given below as a necessary introduction to the theme of this paper.

1.2.1. Total SERR, G

For the purpose of illustration, consider once again Fig. 1 which shows an interfacial crack starting from the "free" edge of a cantilever beam. The beam carries a load of given magnitude acting at a given location. a is the length of the crack. This arrangement is designated as Model 1. Next consider a companion model with a crack length of $a + \Delta a$ with the same load. This is designated as Model 2.

The following potential energy calculations are performed for a given value of P, viz. $\bar{P}$

(i) The potential energy of Model 1, Π_1^0 (State (i)).
(ii) The potential energy of Model 2, Π_2^0 (State (ii)).

The subscripts 1 and 2 correspond to models with crack length a and $a + \Delta a$ respectively. The superscript 0 refers to the fact no constraints are being imposed.

The potential energy is given in terms of external load P and the corresponding deflections δ:

$$\Pi = \int_0^{\bar{\delta}} P(\delta)\mathrm{d}\delta - \bar{P}\bar{\delta} \tag{2}$$

where $\bar{\delta}$ is the displacement corresponding to load $\bar{P}$. The first term gives the strain energy as the work done by external load P as it increases from 0 to $\bar{P}$. The total strain energy release rate, G, is given by:

$$G = \frac{(\Pi_1^0 - \Pi_2^0)}{\Delta a} \tag{3}$$

For a linear problem, G is given by $G = (1/2)\bar{P}\tilde{\delta}$, where $\tilde{\delta}$ gives the difference between the displacements, δ_2 and δ_1 corresponding to $\bar{P}$ of the two models.

1.2.2. Modal components

To find the modal components of G, we go through two complementary sequences of steps. In Sequence I, the potential energies are determined, under the following two conditions:

(iii) The crack tip of Model 1 is conditioned over the length b downstream of the crack, (Fig. 2) to suppress shear mode, by stipulating the relative displacements of the delaminated surfaces to be zero, i.e. $\tilde{u} = 0$.

Compute the potential energy under this condition for the given load, Π_1^1 (State (iii)).

The superscript 1 indicates that crack is conditioned for mode I extension by eliminating $\tilde{u}$.

(iv) Consider now Model 2, with the crack conditioned likewise, but over the length $b + \Delta a$ ($\Delta a = \Delta b$). Compute the potential energy under this condition, Π_2^1 (State (iv)).

These potential energies will give an estimate of strain-energy release rate in mode I, viz. G_{I}^a. Thus we have

$$G_{\mathrm{I}}^a = \frac{(\Pi_1^1 - \Pi_2^1)}{\Delta a} \tag{4a}$$

Note that the superscript a has been introduced to emphasize the approximate nature of this result. This point will be discussed at the close of this section. Now let us visualize that all the constraints are released so

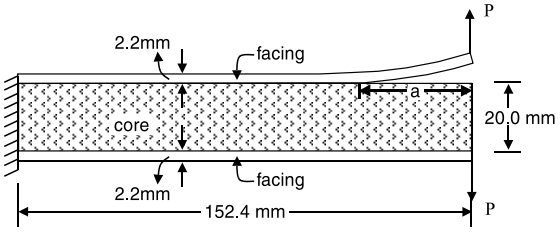

Fig. 2. A double cantilever sandwich beam carrying an interfacial crack.

that the crack surfaces becomes traction free. This completes the Sequence I. (The implications of the release of constraints will be discussed in the next section.)

Let us now consider the complementary sequence of steps, Sequence II, which will yield a similar estimate of SERR in mode II, G^a_{II}. Though the procedure followed is similar, we state it here to introduce the notation that will be useful later on.

(v) Return to Model 1. The crack tip is now conditioned over the same length b downstream of the crack to suppress the opening mode, by setting the relative displacement in the y-direction between the delaminated surfaces to be zero, i.e. $\tilde{v} = 0$.

Compute the potential energy under this condition, Π^2_1 (State (v)).

(vi) Consider Model 2, with the crack conditioned likewise, but over the length $b + \Delta a$.

Compute the potential energy under this condition, Π^2_2 (State (vi)).

Once again, Sequence II becomes complete when all the constraints are released so that the crack becomes traction free.

The modal component G^a_{II} is given by

$$G^a_{II} = \frac{(\Pi^2_1 - \Pi^2_2)}{\Delta a} \tag{4b}$$

We note here, the Sequences I and II by which G^a_I and G^a_{II} are found respectively are two complementary thought experiments. These are artificial processes of crack extension, but will later be found to be useful ways of thinking about the total phenomenon. Note the computed G's are displacement-based and are not controlled by the crack-tip field stresses which are mesh-sensitive. This approach has been applied for delaminated laminates under compression and was found to be far more robust than the stress-based crack-closure integrals especially for bi-material cracks. The former gives values which are mesh-dependent, while the latter were convergent (Johnson and Sridharan, 1999). However the authors have acknowledged that this method is approximate because of the constraints introduced during the process of conditioning a part of the crack downstream of the crack tip. The effects of these constraints are not accounted for in the calculations. Thus the approach involves an error which has not been quantified. Note also the dependence of the results on the distance b over which the crack tip is conditioned has not been investigated. Hence the superscript a, as mentioned earlier.

1.2.3. J-integral

The pathindependent J-contour integral offers an alternative means of computing the total strain energy release rate (Rice, 1968; Anderson, 1995). Since G^a_I and G^a_{II} are the energy release rates with appropriate constraints stipulated over a length b from the crack tip, J-integral can be used to evaluate the same provided the contour meets the crack at a distance less than b. Such an approach has been used Johnson and Sridharan (1999) in their evaluation of the modal components of G. Values thus obtained J^a_I, J^a_{II} were in good agreement G^a_I and G^a_{II} respectively. The evaluation of these parameters is based on numerical analysis and actual experimentation is not contemplated at present.

2. New displacement based approach

2.1. Conceptual basis

2.1.1. Complementary mechanisms

State (iii) can be reached from State (i) by attaching mode II (shear) springs between the delaminated surfaces over the length b from the crack tip and straining them till the relative displacements $\tilde{u}$ vanish. The

work done by the springs $U_{\mathrm{II}}^{(1)}$ accounts for the difference in the potential energies of the two states and is given by: $U_{\mathrm{II}}^{(1)} = \int_0^b \int_0^{\tilde{u}} F_{\mathrm{II}}\,\mathrm{d}\tilde{u}\,\mathrm{d}x$ where F_{II} is the force in the shear springs. Thus we have:

$$\Pi_1^0 = \Pi_1^1 - U_{\mathrm{II}}^{(1)} \tag{5a}$$

The second term in the right-hand side of Eq. (5a), is the strain energy in mode II stored in the springs which when released, the model will revert to its unconstrained state (State (i)).

Similar correspondence exists between States (iv) and (ii). Thus we have

$$\Pi_2^0 = \Pi_2^1 - U_{\mathrm{II}}^{(2)} \tag{5b}$$

where $U_{\mathrm{II}}^{(2)}$ stands for the energies stored in shear springs connecting the delaminated surfaces over the distance $b + \Delta a$ downstream of the new crack tip.

The difference $\Pi_1^1 - \Pi_2^1$ represents the energy released in mode I while the difference $U_{\mathrm{II}}^{(2)} - U_{\mathrm{II}}^{(1)}$ is the energy that is required to eliminate mode II during crack extension. This can be viewed as the mode II energy that must be released after crack extension to achieve traction free crack surfaces, with the corresponding SERR designated as G_{II}^b. Thus we have:

$$G_{\mathrm{II}}^b = \frac{\left(U_{\mathrm{II}}^{(2)} - U_{\mathrm{I}}^{(1)}\right)}{\Delta b} = \frac{\left\{\Pi_2^1 - \Pi_2^0\right\} - \left\{\Pi_1^1 - \Pi_1^0\right\}}{\Delta b} \tag{5c}$$

It is seen by a comparison of Eqs. (3), (4a) and (5c), that

$$G = G_{\mathrm{I}}^a + G_{\mathrm{II}}^b \tag{5d}$$

where G_{II}^b is an estimate of mode II SERR complementary to G_{I}^a as found from Sequence I.

This development is repeated for Sequence II, where the mode II action is restrained over the lengths b and $b + \Delta b$ respectively: State (v) can be reached from State (i) by attaching mode I (normal) springs over a distance b from the crack tip and straining them till the relative displacements $\tilde{v}$ vanish. The work done by the springs $U_{\mathrm{I}}^{(1)}$ accounts for the difference in the potential energies of the two states and is given by:

$$U_{\mathrm{I}}^{(1)} = \int_0^b \int_0^{\tilde{v}} F_{\mathrm{I}}\,\mathrm{d}\tilde{v}\,\mathrm{d}x \tag{6}$$

where F_{I} is the force in the normal spring over the length b. Thus we have:

$$\Pi_1^0 = \Pi_1^2 - U_{\mathrm{I}}^{(1)} \tag{7a}$$

The second term on right-hand side represents energy stored in the normal springs as the relative v's are eliminated between the delaminated surfaces. Similar correspondence exists between States (vi) and (ii). Thus we have:

$$\Pi_2^0 = \Pi_2^2 - U_{\mathrm{I}}^{(2)} \tag{7b}$$

where the second term represents the energies stored in the normal springs over the distance $b + \Delta b$.

Once again, the difference $U_{\mathrm{I}}^{(2)} - U_{\mathrm{I}}^{(1)}$ is the energy stored in the normal springs that is required to eliminate mode I during crack extension. This can be viewed as the mode I energy that must be released after crack extension to achieve traction free crack surfaces. With the corresponding SERR designated as G_{I}^b. Thus we have

$$G_{\mathrm{I}}^b = \frac{\left(U_{\mathrm{I}}^{(2)} - U_{\mathrm{I}}^{(1)}\right)}{\Delta b} = \frac{\left\{\Pi_2^2 - \Pi_2^0\right\} - \left\{\Pi_1^2 - \Pi_1^0\right\}}{\Delta b} \tag{7c}$$

It is seen by a comparison of Eqs. (3), (4b) and (7c), that

$$G = G_{\mathrm{II}}^{a} + G_{\mathrm{I}}^{b} \tag{7d}$$

where G_{II}^{a} and G_{I}^{b} are estimates of mode I and mode II SERR's respectively as found from Sequence II.

2.1.2. Linear combination of the mechanisms

In so far as Sequences I and II are complementary process of constrained crack extension and subsequent release of constraints, the actual process of crack extension should be separable into these processes. (This separation is generally possible provided b is sufficiently large and does not approach zero – a point discussed later in the paper.) Thus the actual fracture process can be viewed as a linear combination of the two processes. Thus linearly combining Eqs. (5d) and (7d), we have:

$$G = n(G_{\mathrm{I}}^{a} + G_{\mathrm{II}}^{b}) + (1-n)(G_{\mathrm{II}}^{a} + G_{\mathrm{I}}^{b}) \tag{8}$$

where n is as yet unknown. Rearranging,

$$G = \left\{nG_{\mathrm{I}}^{a} + (1-n)G_{\mathrm{I}}^{b}\right\} + \left\{(1-n)G_{\mathrm{II}}^{a} + nG_{\mathrm{II}}^{b}\right\} \tag{9}$$

Identifying the first term and the second term on right-hand side as G_{I} and G_{II} respectively, we have

$$G_{\mathrm{I}} = \left\{nG_{\mathrm{I}}^{a} + (1-n)G_{\mathrm{I}}^{b}\right\} \tag{10a}$$

$$G_{\mathrm{II}} = \left\{(1-n)G_{\mathrm{II}}^{a} + nG_{\mathrm{II}}^{b}\right\} \tag{10b}$$

In view of Eqs. (5d) and (7d), these equations can be written in the form:

$$G_{\mathrm{I}} = \left\{nG_{\mathrm{I}}^{a} + (1-n)(G - G_{\mathrm{II}}^{a})\right\} \tag{10c}$$

$$G_{\mathrm{II}} = \left\{(1-n)G_{\mathrm{II}}^{a} + n(G - G_{\mathrm{I}}^{a})\right\} \tag{10d}$$

From Eq. (9) it is clear that G_{I} and G_{II} add up to G.

2.1.3. Determination of n

In Eqs. (10c) and (10d), n can be a function of b, but G_{I} and G_{II} must be independent of b. Thus we can differentiate G_{I} and G_{II} with respect to b as many times as may be warranted and equate the derivatives to zero. Thus we have

$$\frac{\mathrm{d}G_{\mathrm{I}}}{\mathrm{d}b} = 0; \quad \frac{\mathrm{d}^2G_{\mathrm{I}}}{\mathrm{d}b^2} = 0; \quad \frac{\mathrm{d}^3G_{\mathrm{I}}}{\mathrm{d}b^3} = 0; \quad \text{and so on} \tag{11}$$

Since $G_{\mathrm{II}} = G - G_{\mathrm{I}}$ and G is independent of b, it follows:

$$\frac{\mathrm{d}G_{\mathrm{II}}}{\mathrm{d}b} = 0; \quad \frac{\mathrm{d}^2G_{\mathrm{II}}}{\mathrm{d}b^2} = 0; \quad \frac{\mathrm{d}^3G_{\mathrm{II}}}{\mathrm{d}b^3} = 0; \quad \text{and so on} \tag{12}$$

Thus we need to deal with either Eq. (11) or Eq. (12). Differentiating both sides of Eq. (10c) and making use of Eq. (11) we have

$$n\beta' + n'\beta = \gamma \tag{13a}$$

$$n\beta'' + 2n'\beta' + n''\beta = \gamma' \tag{13b}$$

and so on

In the foregoing,

$$\beta = G_{\mathrm{I}}^{a} + G_{\mathrm{II}}^{a} - G \tag{14a}$$

$$\beta' = \frac{\mathrm{d}\beta}{\mathrm{d}b} = \frac{\mathrm{d}G_{\mathrm{I}}^a}{\mathrm{d}b} + \frac{\mathrm{d}G_{\mathrm{II}}^a}{\mathrm{d}b} \tag{14b}$$

$$\beta'' = \frac{\mathrm{d}^2\beta}{\mathrm{d}b^2} \tag{14c}$$

$$\gamma = \frac{\mathrm{d}G_{\mathrm{II}}^a}{\mathrm{d}b} \tag{14d}$$

$$\gamma' = \frac{\mathrm{d}\gamma}{\mathrm{d}b} \tag{14e}$$

$$n' = \frac{\mathrm{d}n}{\mathrm{d}b} \tag{14f}$$

$$n'' = \frac{\mathrm{d}^2 n}{\mathrm{d}b^2} \tag{14g}$$

Thus n and its derivatives can be obtained if the derivatives of G_{I}^a and G_{II}^a are available. This calls for an appropriate integration scheme, which is described in the sequel.

In the present study, we restrict ourselves to the first two of the equations in the sequence, viz. Eqs. (13a) and (13b) as we anticipate the lower order derivatives to be dominant over the higher order ones. The origin is taken at the mouth of the crack, A and the x-axis along the upstream direction of the crack. We select four equispaced station points (A, B, C and D) including the origin (Fig. 1(b)) distant b_1, b_2, b_3 and b_4 respectively from the crack tip, ($a = b_1$). If the corresponding x-coordinates are x_1, x_2, x_3, x_4, then $x_i = a - b_i$. G_{I}^a and G_{II}^a are evaluated on these points with b set equal to b_i.

It is easily seen that the rate of change of G_{I}^a and G_{II}^a must be zero at A, as removing the constraining springs for a infinitesimally short distance from A can affect the neither the stress distribution nor the energy content in the models from St. Venant's principle. (This statement is also verified by several numerical examples run by the author.) Thus β' and γ are both zero at A. Thus $n' = 0$ at A from Eq. (13a) applied at A. In order to proceed further, we assume that the variation of n over the length AB ($= s$) in the form of a Hermitian cubic polynomial in terms of the values of n at A and B and n' at B:

$$n = n_1(1 - 3\eta^2 + 2\eta^3) + n_2(3\eta^2 - 2\eta^3) + n_2' s(-\eta^2 + \eta^3) \tag{15}$$

Here n_1 and n_2 are the values of n at A and B respectively, n_2' is $\mathrm{d}n/\mathrm{d}x$ ($= -\mathrm{d}n/\mathrm{d}b$) at B and $\eta = x/s$. This expression is used to express n'' in terms of n_1, n_2 and n_2' at $\eta = 0, 1$ (i.e. A and B). Forward difference formulae are used to express the derivatives of G_{I}^a and G_{II}^a at A and B in terms of their values at A, B, C and D respectively. Thus the first and second derivatives of a certain function f (which may be G_{I}^a or G_{II}^a) at A can be expressed in terms of the values of f at A, B and C.

$$\left\{\frac{\mathrm{d}f}{\mathrm{d}x}\right\}_{\mathrm{A}} = \frac{f_{\mathrm{B}} - f_{\mathrm{A}}}{s}$$

$$\left\{\frac{\mathrm{d}^2 f}{\mathrm{d}x^2}\right\}_{\mathrm{A}} = \frac{f_{\mathrm{C}} - 2f_{\mathrm{B}} + f_{\mathrm{A}}}{s^2}$$

Similar expressions can be written down for the derivatives at B in terms of the values of f at B, C and D. Thus we set up three equations, invoking Eq. (13b) at A and Eqs. (13a) and (13b) at B. The solution of these equations gives the values of n_1 and n_2 at A and B. Eqs. (10c) and (10d) then gives G_{I} and G_{II}.

The choice of s requires care. It is recommended that the greater of the changes in G_{I}^a and G_{II}^a over the length of $4s$ must be of the order of 1% of G. Too small a change will result in poor results as the resulting equations would then tend to be near-singular and local blips and noises would contaminate the solution;

on the other hand too large a variation will reduce the accuracy of the solution. These points will become apparent by a study of numerical examples presented.

2.1.4. Numerical implementation

For the calculation of G_{I}^{a} and G_{II}^{a}, selective constraints have to be applied between the nodes across the crack; and further there must be facility for changing the length of the crack, a and the length over which the constraints are applied, b. To this end, independent nodes are defined at the top and bottom faces of the entire plane containing the crack. Over the closed uncracked portion the corresponding nodes are tied by two constraints (displacements in two perpendicular directions are set equal to each other for the nodes); and over the portion b, only one of the displacement components is matched. (vide Abaqus Users' manual, Version 5.8, Chapter 20). This arrangement makes it easy to change both a and b.

3. Illustrative examples and discussion

We consider a small number of examples in order to explore the validity and the robustness of the proposed approach.

3.1. Example of a double cantilever beam (homogeneous material)

Consider the double cantilever sandwich beam specimen, fixed at one end and carrying equal and opposite forces ($P = 10$ N) at the extremities of the free edge shown in Fig. 2. The crack length, a, is taken as 25.5 mm.

The dimensions of the specimen are shown in the figure. The specimen is in general, a sandwich beam, a composite made up of isotropic materials, with differing properties for the facing sheets (E_{f}, v) and the core (E_{c}, v) respectively. In order to examine the validity of the new approach, we consider the material to be homogeneous and set $E_{\mathrm{f}} = E_{\mathrm{c}}$ ($E_{\mathrm{f}} = 70\,000$ MPa, $v_{\mathrm{f}} = v_{\mathrm{c}} = 0.33$). In all the cases the crack extension Δa was set equal to, the mesh size $(\tilde{h})$, i.e. the size of the element in the axial direction at the crack tip. Computations were carried out using eight-noded bi-quadratic plane strain elements (CPE8) available in Abaqus (1998).

Table 1 gives the values of G_{I}^{a} and G_{II}^{a} obtained for a certain mesh size $(\tilde{h})$ and s. It is seen that these values remain nearly constant for a certain distance, but then rise sharply towards the crack tip. The computed values of n at A and B and the corresponding values of G_{I} and G_{II} are also shown. It is seen that the latter values are very close as expected. Table 2 gives the results obtained using stress-based crack-closure integrals (G_1 and G_2) and the present displacement-based approach (G_{I} and G_{II}) for three different values of $\tilde{h}$. The total SERR, $G_{\cdot s}$ $(= G_1 + G_2)$ and $G_{\cdot d}$ $(= G_{\mathrm{I}} + G_{\mathrm{II}})$ given the stress-based and displacement-based approaches is almost the same. The values of the modal components given by either of the two approaches (G_1 and G_2 based on crack-closure integrals and G_{I} and G_{II} as given by the present approach) are not palpably sensitive to mesh refinement – a variation of about 3% being observed over the range of $\tilde{h}$ from 0.75 to 0.1 mm. The values of stress-based G_1 and G_2, agree quite closely with G_{I} and G_{II} within a 1–2%. It must be noted however, the values of G_{I} and G_{II} can vary slightly depend upon the type of integration used

Table 1
Typical results for the homogeneous double cantilever problem ($a = 25.5$ mm, $\tilde{h} = 0.1$ mm)

Location	x (mm)	b (mm)	G_{I}^{a}	G_{II}^{a}	n	n'	G_{I} (N/mm)	G_{II} (N/mm)
A	0.0	25.5	0.20177	0.18×10^{-10}	0.5497	0.0	0.3456	0.1756
B	8.4	17.1	0.20177	0.354×10^{-7}	0.5515	0.426×10^{-2}	0.3451	0.1761
C	16.8	8.7	0.20385	0.102×10^{-4}				
D	25.2	0.3	0.32310	0.14155				

Table 2
SERR (N/mm) for the homogeneous double cantilever for varying mesh size

$\tilde{h}$ (mm)	G_1	G_I	G_2	G_{II}
0.75	0.3622	0.3559	0.1727	0.1749
0.25	0.3516	0.3475	0.1717	0.1758
0.10	0.3505	0.3453	0.1708	0.1758

and therefore not much significance must be attached to this discrepancy. It is felt that the values G_I and G_{II} given by the present approach are not exact in any sense of the term but are sufficiently accurate for practical applications.

Table 1 offers a comparison between the values of the approximate displacement-based modal components of G, viz. G_I^a and G_{II}^a and the corrected values, G_I and G_{II} for four different values of b. It is clear that the approximate values can vary over a wide range depending on b – something not reported by Johnson and Sridharan (1999). For the smallest value of b, the approximate values are still in error in excess of 10%.

It is clear that the present procedure is computationally expensive and obviously not warranted for cracks in homogeneous media. However the example lends credence to the new approach and the concepts on which it is based.

3.2. Bi-material crack under mode I loading: Sun's problem

Sun and Jih (1987) considered the problem of a rectangular plate made by joining two rectangular halves each of which is made up of a material different from the other. The plate carries a crack located at the center, along the interface of the two materials (Fig. 3). The material properties are given as E_1 and v_1 for material 1 and E_2 and v_2 for material 2 respectively.

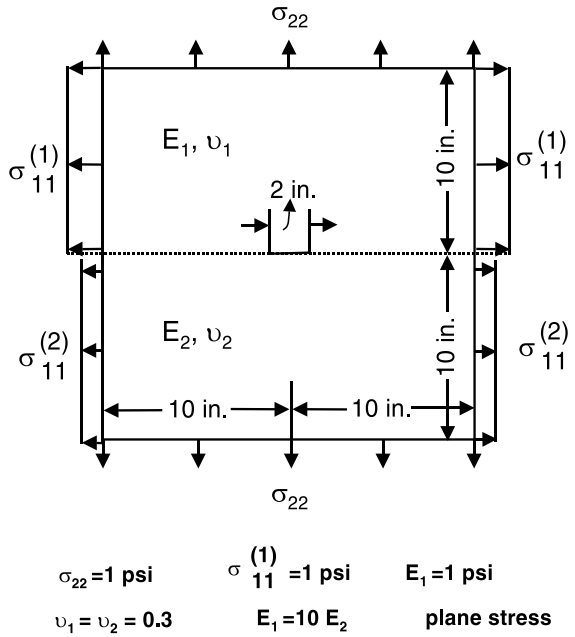

Fig. 3. Geometry, material properties and loading conditions for a square panel with a central crack along the bi-material interface.

The plate carries uniform normal stress σ_{22} applied at the boundaries parallel to the crack, and uniform stresses $\sigma_{11}^{(1)}$ and $\sigma_{11}^{(2)}$ in parts (1) and (2) respectively, in the perpendicular direction; the ratio of these stresses is so computed that the transverse strains ϵ_{11} will be the same in the two plates in the uncracked plate. Only one half the plate is analyzed because of symmetry. For mode separation analysis by the present approach, we set $b = a$, $3a/4$, $a/2$ and $a/4$ respectively for the calculation of G_{I}^{a} and G_{II}^{a}. The calculations were repeated for several values of $\tilde{h}$ (with $\Delta a = \tilde{h}$) to study the convergence of the solution. Eight-noded plane stress elements (CPS8) were employed in the analysis.

Fig. 4 shows the present results along with those of Sun and Jih. The present model gives results which gently oscillate over a small range, but the results do give a much higher value for G_{I} and correspondingly a small value for G_{II} consistently. The results do make sense as in this problem there is little tendency for shearing stresses to develop at the interface. The result given by the stress-based approach for very refined meshes, is $G_{\mathrm{I}} = G_{\mathrm{II}}$ which is clearly counter-intuitive.

Table 3 illustrates computational features of the problem for a certain value of $\tilde{h}$, viz. 0.01 in. It is interesting to see that while G_{I}^{a} decreases with b slightly, G_{II}^{a} increases from zero to a value which is of the order of 1% of G over the range considered. The table also values of J's computed for crack lengths of a and $a + \Delta a$ respectively, for every b considered. These values of G's lie right in between these values of J.

Once again it is clear the proposed approach is computationally expensive for routine applications. However the results given by this approach are close to those given by crack-closure integrals for

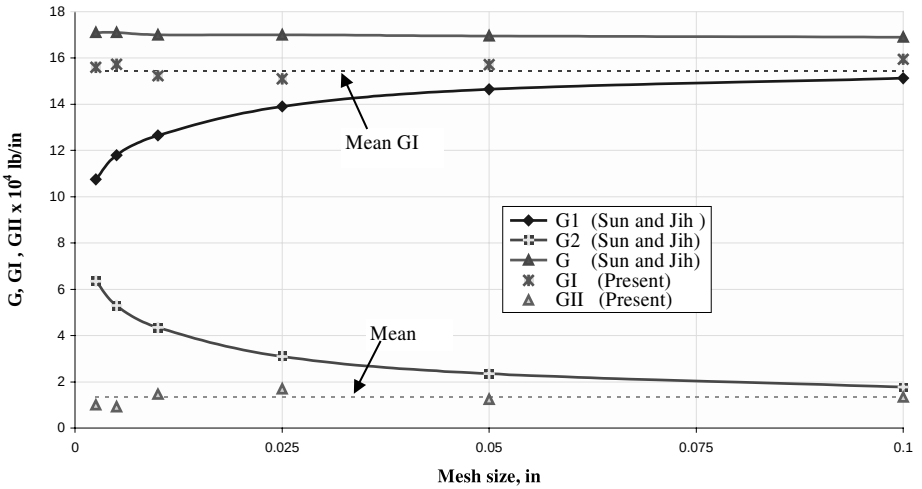

Fig. 4. The strain energy release rate and its components versus mesh size.

Table 3
Typical results for Sun's problem: $\tilde{h} = 0.01$ in., $G = 0.1669 \times 10^{-2}$

b (mm)	$G_{\mathrm{I}}^{a} \times 10^{-2}$	$G_{\mathrm{II}}^{a} \times 10^{-2}$	$J_{\mathrm{I}}^{a} \times 10^{-2}$	$J_{\mathrm{II}}^{a} \times 10^{-2}$	n	dn/db	G_{I}	G_{II}
1.0	0.16127	0.0	0.1605/0.1621	0.0	2.59	0.0	0.1523	0.0146
0.75	0.16126	0.155×10^{-4}	0.1605/0.1621	$0.155 \times 10^{-4}/0.155 \times 10^{-4}$	2.60	0.07	0.1523	0.0146
0.5	0.16113	0.288×10^{-3}	0.1603/0.1620	$0.293 \times 10^{-3}/0.283 \times 10^{-3}$				
0.25	0.16010	0.208×10^{-2}	0.1593/0.1610	$0.213 \times 10^{-2}/0.203 \times 10^{-2}$				

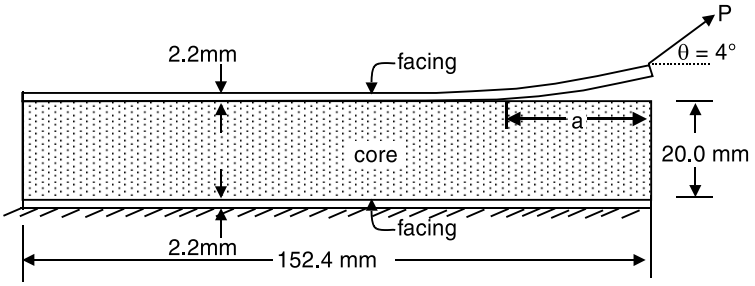

Fig. 5. A "tilted sandwich beam" specimen carrying a load P acting at an angle of 4°.

a relatively coarse mesh – the results that are thought to be close to reality (Sun and Jih, 1987; Rice, 1968).

3.3. Bi-material crack exhibiting mode-mixity

A sandwich specimen with the same geometry as in example 1 is selected. The modulus of elasticity of the core material is taken as 1% of that the facing sheet ($E_f/E_c = 0.01$, $E_f = 70{,}000$ MPa, $v_f = v_c = 0.3$), to provide a strong bi-materiality to the specimen. A crack of 25.5 mm length is considered between the facing sheet and the core. The bottom of the specimen fully restrained and a tensile load of 25 N acting at an inclination of 4° to the axis of the specimen, is applied at the top tip of the delaminated portion of the facing sheet. (Fig. 5) The angle is so chosen as to avoid contact between the delaminated surfaces and to provide a sizeable mode-mixity. Note that similar specimens have been used by Li and Carlsson (1999) in their experimental investigation of interfacial fracture toughness.

Fig. 6 shows the variation of G, G_I and G_{II} as obtained by the stress-based and the present displacement approaches respectively. A spectrum of mesh sizes near the crack tip is considered, from $\tilde{h} = 0.025$ to 0.75

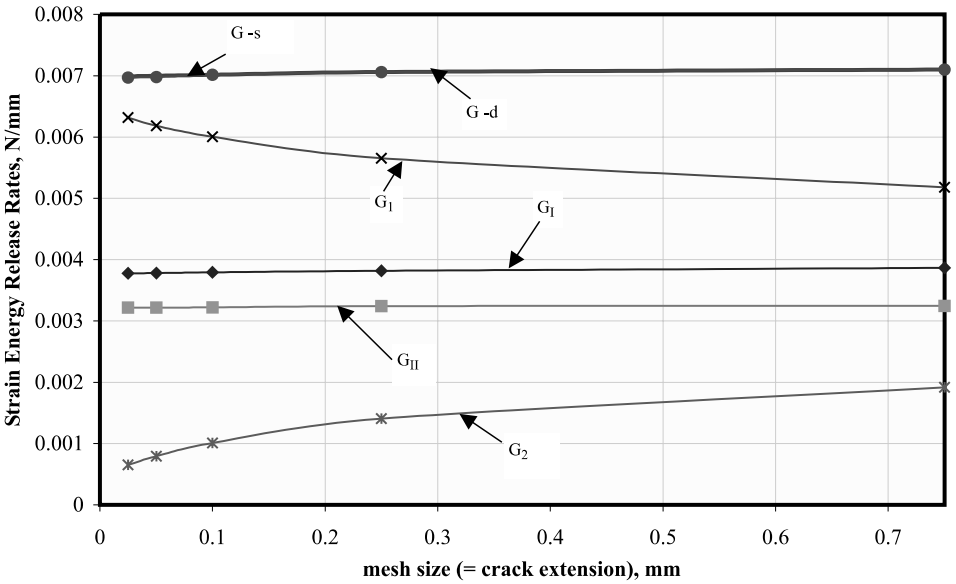

Fig. 6. Variation of $G_1 - G_2$ and $G_I - G_{II}$ with mesh size.

Table 4
Typical results for the tilted sandwich problem: $\tilde{h} = 0.05$ mm, $G = 6.9992 \times 10^{-3}$

Location	x (mm)	b (mm)	$G_{\mathrm{I}}^{a} \times 10^{-3}$ (N/mm)	$G_{\mathrm{II}}^{a} \times 10^{-3}$ (N/mm)	n	n'	$G_{\mathrm{I}} \times 10^{-3}$ (N/mm)	$G_{\mathrm{II}} \times 10^{-3}$ (N/mm)
A	0.0	25.5	2.9860	2.2452	0.54	0.0	3.801	3.198
B	6.0	19.5	2.9891	2.2703	0.55	0.00344	3.781	3.218
C	12.0	13.5	3.0650	2.2833				
D	18.0	7.5	3.3692	2.5221				

mm. For all calculations, we set $\Delta a = \tilde{h}$. For the calculation of the displacement-based G_{I} and G_{II}, we select A, B, C, D at a spacing, $s = 6$ mm. Table 4 gives the typical data obtained for certain value of $\tilde{h}$ (= 0.05 mm).

It is clearly seen from the Fig. 6, in the range of mesh refinement considered viz. the stress-based G_1 and G_2 show no tendency to converge, though the total G is clearly convergent and agrees with the displacement-based G completely. On the other hand, the displacement-based G_{I} and G_{II} change very little with mesh refinement and provide consistent values.

Fig. 7 shows the values of G_{I}^{a} and G_{II}^{a} obtained using a fine mesh ($\tilde{h} = 0.05$ mm) for various values of b. The corrected values, G_{I} and G_{II} are also indicated alongside. The former do differ significantly from the latter and vary rapidly as $b \Rightarrow 0$. In this range, the rates of change of G_{I}^{a} and G_{II}^{a} are roughly equal and opposite to each other and G_{I}^{a} and G_{II}^{a} sum up to G. This would make both β, $\beta' \Rightarrow 0$ rendering Eqs. (13a) and (13b) nearly singular. Though it is not certain that such behavior is typical at the crack tip in every bi-material problem, it is recommended no station points at which n and n' is evaluated (i.e. A and B) should be defined too close to the crack tip.

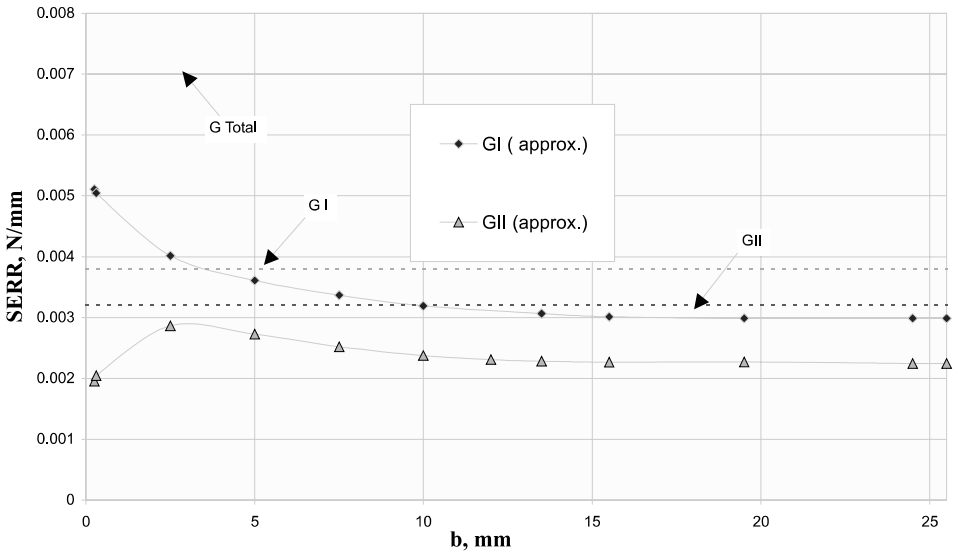

Fig. 7. Variation of G_{I}^{a} and G_{II}^{a} with respect to b (mesh size $\tilde{h} = \Delta a = 0.05$ mm).

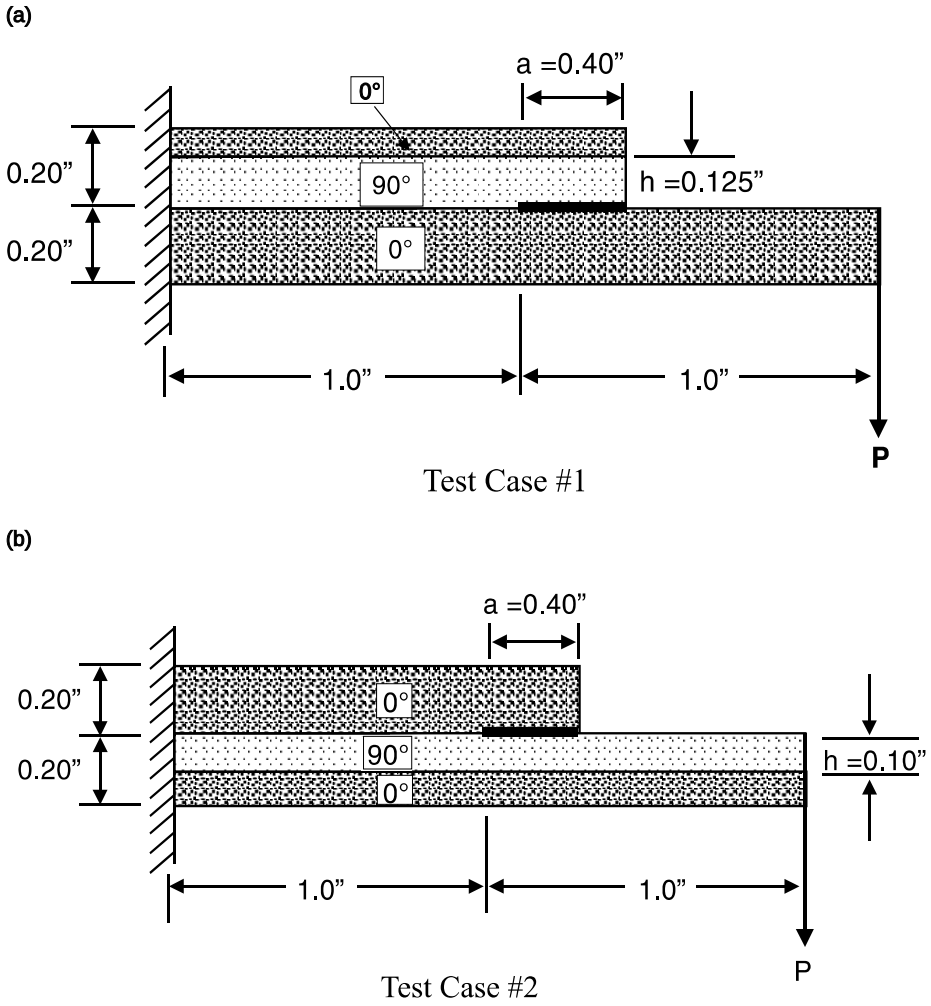

Fig. 8. (a) Geometry and loading of Beuth's [9] test case #1. (b). Geometry and loading of Beuth's [9] test case #2.

Table 5
Graphite-epoxy ply properties used in test cases (all modulii are in lb/in^2)

Elastic constants	Values
E_{11}	19.5×10^6
$E_{22} = E_{33}$	1.48×10^6
$G_{12} = G_{13}$	0.80×10^6
G_{23}	0.497×10^6
$v_{12} = v_{13}$	0.30
v_{23}	0.49

Note: Subscripts 1, 2 and 3 refer to the direction along the fiber, the inplane direction transverse to the fiber and the out-of-plane direction normal to the fiber respectively.

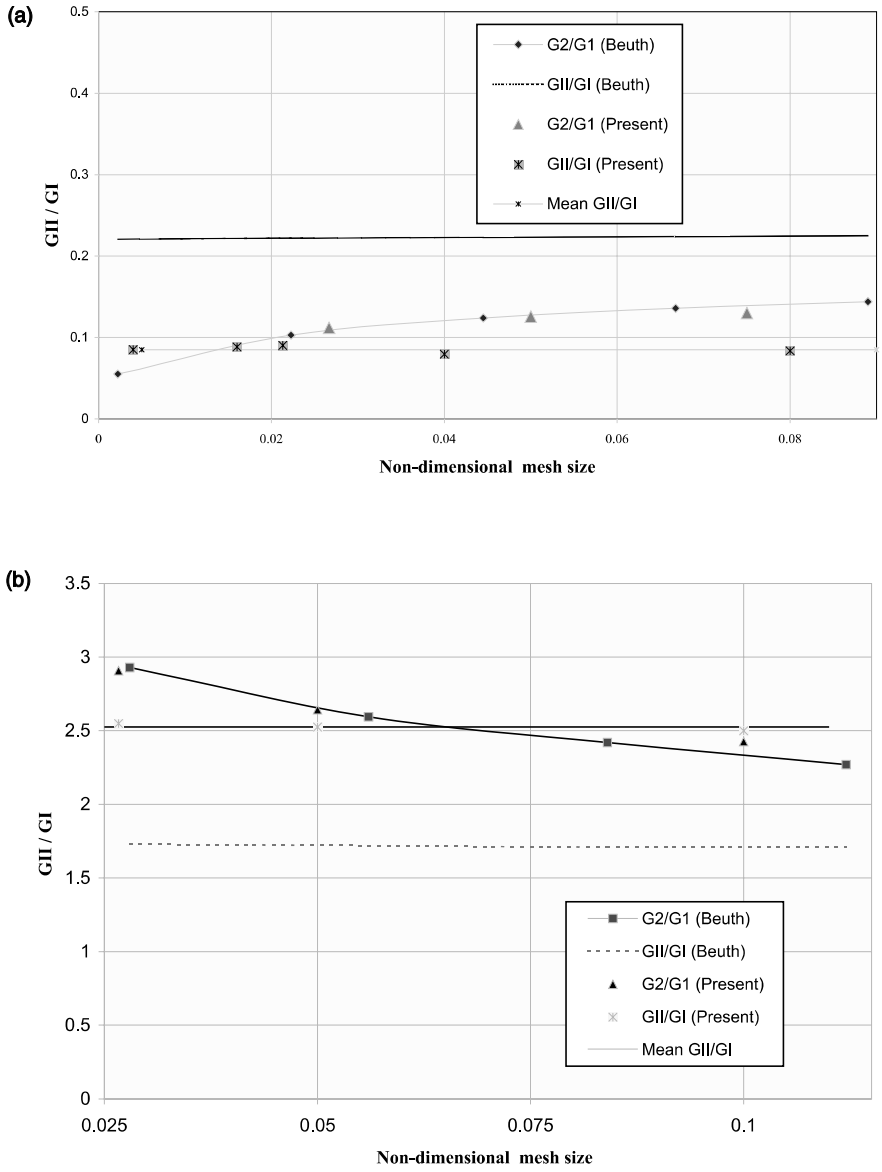

Fig. 9. (a) Mode-mixity ratio (G_{II}/G_I) versus normalized crack extension length for test case #1. (b) Mode-mixity ratio (G_{II}/G_I) versus normalized crack extension length for test case #2.

3.4. Beuth problem of layered orthotropic composites

Beuth (1996) investigated two problems which are shown in Fig. 8(a) and (b) and these will be referred to as test cases #1 and #2 respectively. The two cases consist of plane strain drop-ply configurations of 0° and 90°, 0.005 in. thick graphite epoxy plies. The displacements are fully constrained on the left edge in each case. On the right-hand side a lateral concentrated load of P (taken as 120 lb, in the calculations) is applied at the bottom tip of the bottom ply. The properties of the plies with respect to their material principal axes are given in Table 5.

The results obtained for the two cases are plotted in Fig. 9(a) and (b) respectively. The results are in the form of ratios of G_2/G_1 obtained by crack-closure integrals, the present displacement-based approach ($\Delta a = \tilde{h}$, s varying from 0.1 to 0.2 mm) and Beuth's technique of mode separation, all plotted with respect to the nondimensional mesh size, $\tilde{h}/h$, where $h = 0.125$ and 0.1 in. for the two test cases respectively. The crack-closure integrals as obtained by the somewhat simple mesh configuration of the present study and the more elaborate one of Beuth give substantially the same results. However the values of modal ratio G_{II}/G_I as given by the present approach are very different from those of Beuth. The essential concept involved in Beuth's approach is to extract and eliminate the oscillatory part of stress variation near the crack tip in the computation of the SERR. This approach does lead to a consistent projection of the components of SERR, but the validity of the results is by no means established. On the other hand, the displacement based approach has a clear physical meaning and it is therefore believed that it gives the correct values of the modal components of G. Note once again the mode-mixity given by the stress-based approach and the present displacement-based approach respectively are close to each other, provided the mesh employed is not unduly refined.

4. Conclusions

A new displacement-based technique of mode separation of strain energy release rate, G, of interfacial crack growth is presented. The method is applicable for bi-material cracks for which the crack-closure integrals are, in principle, not applicable. The method does correct for the deficiencies in an earlier and simpler presentation of the same. The modal components thus determined do add up to the total value of G and are derived by insisting G_I and G_{II} are independent of b. The method does not depend explicitly on the stress-distribution at the crack tip, is by and large insensitive to mesh refinement and gives results which are in accord with physical intuition. From the examples studied, a mesh size of 5% of the crack length appears sufficient for the evaluation of the modal components.

The method, however, is computationally expensive as it requires the calculation of the approximate values of the modal components at at least four selected station points along the crack line. Perhaps, the most interesting conclusion of the investigation is that the modal components thus found do not differ substantially from those obtained from crack-closure integrals obtained using a relatively coarse mesh.

Acknowledgements

The author was supported by grant from the Office of Naval Research (ONR grant # N00014-91-J-1637) during this investigation. Dr. Yapa D. S. Rajapakse was the Scientific program monitor. Author wishes to thank Mr. Aaron J. McConnell, graduate student (1998–99) at Washington University for his assistance in computation in the early stages of the investigation.

References

ABAQUS, Version 5.8, 1998. Hibbit, Karlsson and Sorenson, Inc., Pawtucket, RI.

Anderson, T.L., 1995. Fracture Mechanics, Fundamentals and Applications, second ed. CRC Press, Boca Raton, FL.

Atkinson, C., 1977. On stress singularities and interfaces in linear fracture mechanics. Int. J. Fract. 13, 807–820.

Beuth, J.L., 1996. Separation of crack extension modes in orthotropic delamination models. Int. J. Fract. 77, 305–321.

Davidson, B.D., 1994. Energy release rate determination of edge delamination under combined in-plane, bending and hygrothermal loading. Part I – delamination at a single interface. J. Comp. Mater. 28, 1009–1031.

Irwin, G.R., 1957. Analysis of stresses and strains near the end of a crack traversing a plate. J. Appl. Mech. 24, 361–364.

Johnson, M.J., Sridharan, S., 1999. Evaluation of strain energy release rates in delaminated laminates under compression. AIAA J. 37, 954–963.

Li, X., Carlsson, L.A., 1999. The tilted sandwich debond TSD specimen for face/core interface fracture characteristics. J. Sandwich Struct. Mater. 1, 60–75.

Raju, I.S., Crews Jr., J.H., Aminpour, M.A., 1998. Convergence of strain energy release rate components for edge-delaminated composite laminates. Engng. Fract. Mech. 30, 383–396.

Rice, J.R., 1968. A path independent integral and the approximate analysis of strain concentration by notches and cracks. J. Appl. Mech. 35, 379–386.

Rybicki, E.F., Kanninen, M.F., 1977. A finite element calculation of stress intensity factors by modified crack closure integral. Engng. Fract. Mech. 9, 931–938.

Sun, C.T., Jih, C.J., 1987. On strain energy release rates for interfacial cracks in bi-material media. Engng. Fract. Mech. 28, 13–20.